PERGAMON

International Journal of Solids and Structures 36 (1999) 1129–1147

INTERNATIONAL JOURNAL OF SOLIDS and STRUCTURES

Two-dimensional linear elasticity by the boundary node method

Vasanth S. Kothnur[a], Subrata Mukherjee[b]*, Yu Xie Mukherjee[c]

[a]*Sibley School of Mechanical and Aerospace Engineering, Cornell University, Ithaca, NY 14853, U.S.A.*
[b]*Department of Theoretical and Applied Mechanics, Cornell University, Ithaca, NY 14853, U.S.A.*
[c]*Dehan Engineering Numerics, 95 Brown Road, Box 1016, Ithaca, NY 14853, U.S.A.*

Received 31 January 1997; and in revised form 24 November 1997

Abstract

This paper presents a further development of the Boundary Node Method (BNM) for 2-D linear elasticity. In this work, the Boundary Integral Equations (BIE) for linear elasticity have been coupled with Moving Least Square (MLS) interpolants; this procedure exploits the mesh-less attributes of the MLS and the dimensionality advantages of the BIE. As a result, the BNM requires only a nodal data structure on the bounding surface of a body. A cell structure is employed only on the boundary in order to carry out numerical integration. In addition, the MLS interpolants have been suitably truncated at corners in order to avoid some of the oscillations observed while solving potential problems by the BNM (Mukherjee and Mukherjee, 1997a). Numerical results presented in this paper, including those for the solution of the Lamé and Kirsch problems, show good agreement with analytical solutions.

1. Introduction

Mesh generation, for traditional Finite Element Method (FEM) analysis of 3-D bodies of complex irregular shape, can prove to be arduous, time consuming and expensive. This is especially true for problems such as shape optimization, modeling of certain manufacturing processes or fracture mechanics with growing cracks, in which remeshing must be carried out several times during an analysis. Hence, there is considerable recent interest in mesh-less methods (see, for example, the review article by Belytschko et al., 1996, as well as other articles, in this special issue of the journal *Computer Methods in Applied Mechanics and Engineering*, devoted to this subject). An ideal situation, perhaps, is a method of analysis that can directly use a solid model for a 3-D object with little or no meshing. The Boundary Node Method (BNM) offers such a possibility.

* Corresponding author.

0020–7683/99/$ - see front matter
PII: S0020–7683(97)00363–6

An important step towards mesh-less methods is the Diffuse Element Method (DEM) proposed by Nayroles et al. (1992). These authors have proposed the coupling of a nodal interpolation scheme, called Moving Least Squares (MLS) interpolants, with Galerkin procedures. In the MLS interpolation scheme, interpolants are fit to nodal values by a least-squares approximation scheme. It is important to mention here that MLS interpolants had been proposed earlier for curve and surface fitting (see, for example Lancaster and Salkauskas, 1990). The DEM only needs a distribution of nodes (points) inside and on a body, and a boundary description, in order to develop the Galerkin equations.

Belytschko and his co-workers have refined and modified the DEM and have called it the Element-Free Galerkin (EFG) method. One of their key contributions has been the introduction of an underlying cell structure for numerical integration. The EFG essentially divorces nodes from elements in the sense that the unknowns, in a discretized problem, are only defined at nodes (points) inside a body, while conventional elements are replaced by cells that are not directly related to the nodal unknowns, but are only necessary for numerical integration. These cells can be very simple and need not satisfy the usual compatibility requirements of conventional finite elements. They can be easily generated inside a computer code and can be easily refined in a local region without modifying them in the rest of the body. Belytschko and his co-workers have advanced the EFG method with great energy and have applied it to a variety of 2-D problems such as potential theory and linear elasticity (Belytschko et al., 1994a), fracture mechanics with crack growth (Belytschko et al., 1994b, 1995a), dynamic fracture (Belytschko et al., 1995b, Belytschko and Tabbara, 1996), plate bending (Krysl and Belytschko, 1995) and shell theory (Krysl and Belytschko, 1996). Preliminary 3-D results for an elastodynamics problem are presented in Belytschko et al. (1996).

The Boundary Element Method (BEM, see example, Mukherjee, 1982; Banerjee, 1994) has a well known dimensionality advantage for linear problems in the sense that, although meshing is required in the conventional manner, only the 2-D bounding surface of a 3-D body needs to be discretized in a numerical solution procedure. The idea of combining the MLS interpolation scheme with Boundary Integral Equations (BIE) is intriguing since such an approach would retain the mesh-less attribute of the former and the dimensionality advantage of the latter. Such a method could then directly employ a solid model of a 3-D body with nodes and cells only on the surface of the body—the so called "salted potato" data structure as shown in Fig. 1a (Mukherjee and Mukherjee, 1997a). This figure shows boundary nodes, denoted by points, as well as cells. The cells, used for integration, must cover the surface of the body as in the standard BEM. The cell structure, however, is much more flexible than the element structure in the BEM in the sense that one or more of a group of cells can be subdivided without affecting the rest of the cells. Also, the number of nodes in each cell is arbitrary, although it appears (see Mukherjee and Mukherjee, 1997b) it is a good idea to use a small number of nodes per cell. This combination of MLS interpolants with the BIE has been recently carried out. The resulting method is called the Boundary Node Method (BNM). Results for 2-D problems in potential theory are presented in Mukherjee and Mukherjee (1997a) and are most encouraging.

A difficulty associated with the use of MLS interpolants is the accurate satisfaction of boundary conditions since these interpolants lack the usual delta function property of conventional shape functions. Belytschko and his co-workers have employed various approaches in order to accurately enforce essential boundary conditions in the EFG method. These ideas include Lagrange multipliers

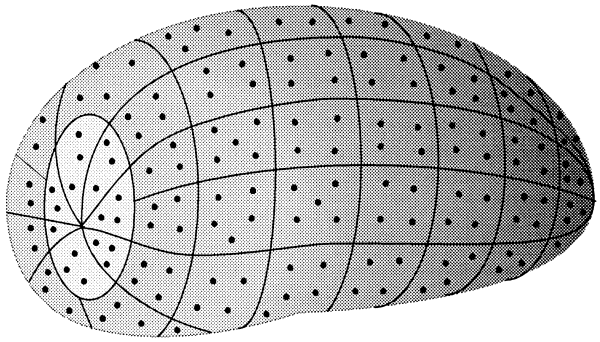

Fig. 1a. Input data structure for the BNM—the salted potato.

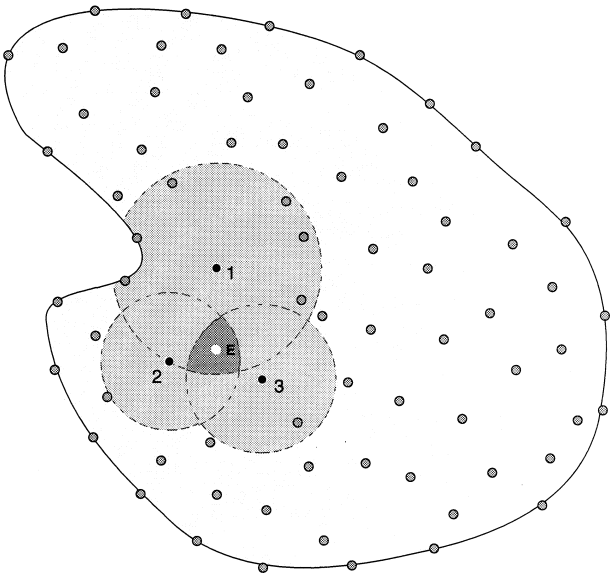

Fig. 1b. Domain of dependence of an evaluation point E.

(Belytschko et al., 1994a), use of tractions as Lagrange multipliers (Lu et al., 1994), collocation (Belytschko and Tabbara, 1996) and coupling of the EFG with finite elements (Krongauz and Belytschko, 1996). A simple and very promising idea, involving a re-definition of the usual discrete norm (used in MLS interpolation) in terms of approximations to the nodal variables, together with post-processing of these approximations, has led to very accurate numerical results in 2-D potential theory (Mukherjee and Mukherjee, 1997b). Another recently proposed remedy, using singular weight functions, is due to Kaljevic and Saigal (1997).

Use of MLS interpolants can lead to difficulties in accurate enforcement of both essential and natural boundary conditions in the BNM. This difficulty has been overcome in Mukherjee and Mukherjee (1997a) by coupling the linear system of equations from the discretized BIE, in terms

of approximations to the nodal variables, together with the discretized forms of the equations that relate these approximations to their actual values (through MLS shape functions). An analogous strategy is employed in the work reported in the present paper.

Another difficulty with the BNM is associated with interpolation of tractions across corners. While displacements in elasticity problems are continuous on the boundary of a body, tractions are typically discontinuous across corners. The shape functions for MLS interpolants, however, are smooth within the domain of dependence of an evaluation point. In Mukherjee and Mukherjee (1997a), domains of dependence were allowed to extend across corners. This approach of approximating discontinuous variables with continuous basis functions led to oscillations in some of the numerical results presented in that paper. In the present work, two strategies, namely domains of dependence that reach across corners, and those that are truncated at corners, are compared in the case of linear elasticity. Although some artifacts (kinks) sometimes remain, the numerical solutions from the latter strategy seem to outperform those from the former. Please see Belytschko et al. (1996) for a discussion of modeling of discontinuities in the EFG method.

The primary contribution of the present paper is the coupling of MLS interpolants with the 2-D BIE for linear elasticity. Another important contribution is the implementation of truncated domains of dependence mentioned above.

This paper is organized as follows. MLS interpolants and weight functions are presented first. This is followed by a brief description of the well known BIE for linear elasticity, first derived by Rizzo (1967). The next section is concerned with imposition of boundary conditions in the elasticity BNM, followed by a discussion of interpolation of discontinuities in tractions across corners. Finally, numerical results for several illustrative 2-D problems, including the classical problems first solved by Lamé and Kirsch, are presented. The computed solutions are in good agreement with the analytical ones.

2. MLS Interpolation scheme for the 2-D BNM

In contrast to the Element Free Galerkin Method, the Moving Least Square interpolants in the BNM are defined on the 1-D bounding surface ∂B of a 2-D body B. As in the usual BEM formulation, the MLS interpolants for each component of displacement and traction can be constructed independently. The MLS interpolants for the displacements $u^{(1)}$, $u^{(2)}$ and tractions $\tau^{(1)}$, $\tau^{(2)}$ are defined as

$$u^{(i)}(s) = \mathbf{p}^T(s)\mathbf{a}^{(i)}(s) \tag{1}$$

$$\tau^{(i)}(s) = \mathbf{p}^T(s)\mathbf{b}^{(i)}(s) \tag{2}$$

where s is a curvilinear coordinate on ∂B, $p_1 = 1$ and $p_j(s)$ $(j = 2, 3, \ldots, m)$ are monomials in s. The monomials $p_j(s)$ provide the intrinsic polynomial bases for $u^{(i)}$ and $\tau^{(i)}$. In the numerical implementation presented later in this paper, a quadratic background basis ($m = 3$) is used, i.e.

$$\mathbf{p}^T(s) = [1, s, s^2] \tag{3}$$

The coefficients $\mathbf{a}^{(i)}(s)$ and $\mathbf{b}^{(i)}(s)$ are obtained by minimization of weighted L_2 norms defined as:

$$J_1^{(i)} = \sum_{I=1}^{n} w(s-s_I)[\mathbf{p}^T(s_I)\mathbf{a}^{(i)}(s) - \hat{u}_I^{(i)}]^2 \tag{4}$$

$$J_2^{(i)} = \sum_{I=1}^{n} w(s-s_I)[\mathbf{p}^T(s_I)[\mathbf{b}^{(i)}(s) - \hat{\tau}_I^{(i)}]^2 \tag{5}$$

where s_I are boundary nodes on ∂B, s is the coordinate of an evaluation point E on ∂B and n is the number of boundary nodes in the neighborhood of E for which the weight function does not vanish at E. As shown in Fig. 1b, the value of a function at an evaluation point E is determined entirely from those nodes which are within its domain of dependence. In this figure, the gray circles denote the ranges of influence of the nodes 1, 2 and 3, while the union of these circles is the domain of dependence of the evaluation point E. Any part of a circle lying outside the body is ignored. The construction of weight functions is discussed int he next section of this paper. As defined in Mukherjee and Mukherjee (1997a), $\hat{u}_I^{(i)}$ and $\hat{\tau}_I^{(i)}$ are approximations to the actual nodal values $u^{(i)}(s_I)$ and $\tau^{(i)}(s_I)$, respectively. The distinctions between $(u_I^{(i)}, t_I^{(i)})$ and $(\hat{u}_I^{(i)}, \hat{\tau}_I^{(i)})$ become necessary because the MLS interpolants lack the delta function property (Mukherjee and Mukherjee, 1997a, b). The quantities $\hat{u}_I^{(i)}$ and $\hat{\tau}_I^{(i)}$ are eventually determined from the BIE and boundary conditions as discussed later in Section 5 of this paper.

The least squares minimization are necessary in order to determine $\mathbf{a}^{(i)}$ and $\mathbf{b}^{(i)}$ which are now functions of the position s. (They are constants in the standard BIE.) Typically, m, the order of the polynomial basis employed (here $m = 3$), is much less than the number of nodes n in the domain of dependence of an evaluation point (here $n > 6$). This situation provides flexibility to both the EFG and the BNM. Nayroles et al. (1992) have shown that the method fails if $n < m$ since the matrix A [defined in eqn (8)] becomes singular in this case. As in Mukherjee and Mukherjee (1997a), the evaluation point can be either a source point P (a boundary node on ∂B) or a field point Q (a regular Gauss or a log weighted Gauss point on ∂B).

Minimizing $J_1^{(i)}$ with respect to $\mathbf{a}^{(i)}(s)$ and $J_2^{(i)}$ with respect to $\mathbf{b}^{(i)}(s)$ $(i = 1, 2)$ lead to:

$$\mathbf{a}^{(i)}(s) = \mathbf{A}^{-1}(s)\mathbf{B}(s)\hat{\mathbf{u}}^{(i)} \tag{6}$$

$$\mathbf{b}^{(i)}(s) = \mathbf{A}^{-1}(s)\mathbf{B}(s)\hat{\boldsymbol{\tau}}^{(i)} \tag{7}$$

where

$$\mathbf{A}(s) = \sum_{I=1}^{n} w(s-s_I)\mathbf{p}(s_I)\mathbf{p}^T(s_I) \tag{8}$$

$$\mathbf{B}(s) = [w_1(s)\mathbf{p}(s_1), w_2(s)\mathbf{p}(s_2), \ldots, w_n(s)\mathbf{p}(s_n)] \tag{9}$$

$$w_I(s) = w(s-s_I) \tag{10}$$

$$\hat{\mathbf{u}}^{(i)} = [\hat{u}_1^{(i)}, \hat{u}_2^{(i)}, \ldots, \hat{u}_n^{(i)}]^T \tag{11}$$

$$\hat{\boldsymbol{\tau}}^{(i)} = [\hat{\tau}_1^{(i)}, \hat{\tau}_2^{(i)}, \ldots, \hat{\tau}_n^{(i)}]^T \tag{12}$$

Therefore the actual nodal values of displacement and traction components can be interpolated in terms of their approximate nodal values by substituting (6) and (7) in (1) and (2), respectively. The results are:

$$u^{(i)}(s) = \mathbf{p}^T(s)\mathbf{A}^{-1}(s)\mathbf{B}(s)\hat{\mathbf{u}}^{(i)} \tag{13}$$

$$\tau^{(i)}(s) = \mathbf{p}^T(s)\mathbf{A}^{-1}(s)\mathbf{B}(s)\hat{\boldsymbol{\tau}}^{(i)} \tag{14}$$

Equations (13) and (14) can be rewritten as

$$u^{(i)}(s) = \sum_{I=1}^{n} \Phi_I(s)\hat{u}_I^{(i)} \tag{15}$$

$$\tau^{(i)}(s) = \sum_{I=1}^{n} \Phi_I(s)\hat{\tau}_I^{(i)} \tag{16}$$

where Φ_I are analogous to the usual shape functions. Note that the same set of shape functions are used to interpolate each component of displacement and traction as in the usual BEM. In this work, s is the local relative coordinate of the boundary point with respect to the evaluation point. Thus, the origin of the local coordinate system is at the evaluation point. Moving in an anti-clockwise direction, s is positive if the boundary point is ahead of the evaluation point and s is negative if the boundary point is behind the evaluation point. Therefore, s for an evaluation point is always zero and $p_1 = 1$, $p_2 = 0$, $p_3 = 0$. For further details of implementation of this procedure, refer to Mukherjee and Mukherjee (1997a). A significant fraction of the total CPU time is spent in the computation of these shape functions.

3. Weight functions

The choice of weight functions for the Element-Free Galerkin Method has been investigated by several investigators (e.g. Nayroles et al., 1992; Belytschko et al., 1994a). As shown in Lancaster and Salkauskas (1981), the shape function $\phi_I(s)$ and its derivatives are continuous upto the same order as the weight function $w_I(s)$ and its derivatives. The weight function chosen in this work is an exponential function, i.e.

$$w_I(s) = \begin{cases} \dfrac{e^{-(d_I/c)^2} - e^{-(\hat{d}_I/c)^2}}{1 - e^{-(\hat{d}_I/c)^2}} & \text{if } d_I \leqslant \hat{d}_I; \\ 0 & \text{if } d_I \geqslant \hat{d}_I \end{cases}. \tag{17}$$

Here, $\hat{d}_I$ is the size of the support of the weight function w_I and it determines the range of influence $\mathscr{R}_s$ of the boundary node s_I. The constant c controls the rate of decay of the weight function. In the numerical implementation presented later, the parameters in the weight function are chosen such that

(a) The number of nodes in the domain of dependence of an evaluation point is in the range 6–12.
(b) The weight function at the farthest node is $\leqslant 0.01$.
(c) The ratio $(c/\hat{d}_i)$ is typically in the range (0.35–0.75) in order to obtain a "reasonable" decay in the weight function.

Note that these parameters can vary over different parts on the body depending on the local cell

density. However, determining an "optimal" distribution, that represents the most efficient or accurate way of constructing the weight functions for a given problem, requires more study.

4. Boundary integral equations for linear elasticity

The well known regularized BIE (Rizzo, 1967 first presented the original form without regularization) for the solution of the governing equations of linear elasticity in a 2-D domain B bounded by ∂B, is given by

$$\int_{\partial B} \{\tau^{(i)} U_{ij}(P,Q) - T_{ij}(P,Q)[u^{(i)}(Q) - u^{(i)}(P)]\}\, \mathrm{d}s_Q = 0 \tag{18}$$

$$U_{ij} = \frac{-1}{8\pi(1-\nu)\mu}\left[(3-4\nu)\delta_{ij}\ln(r) - \frac{y_i y_j}{r^2}\right] \tag{19}$$

$$T_{ij} = \frac{-1}{4\pi(1-\nu)r^2}\left[(1-2\nu)(n_j y_i - n_i y_j) + \left((1-2\nu)\delta_{ij} + \frac{2y_i y_j}{r^2}\right) y_k n_k\right] \tag{20}$$

where U_{ij} and T_{ij} are the usual kernels as in Mukherjee (1982), P and Q are the source and field point, respectively, on ∂B, μ is the shear modulus ν is the Poisson's ratio, δ_{ij} is the Kronecker delta, $y_i = x_i(Q) - x_i(P)$ and (n_1, n_2) are the components of the normal to the boundary at Q. Substituting eqns (15) and (16) in (18) yields

$$\int_{\partial B} \left\{ U_{ij}(P,Q) \sum_{I=1}^{n_Q} \Phi_I(Q)\hat{\tau}_I^{(i)} - T_{ij}(P,Q)\left(\sum_{I=1}^{n_Q} \Phi_I(Q)\hat{u}_I^{(i)} - \sum_{I=1}^{n_P} \Phi_I(P)\hat{u}_I^{(i)}\right)\right\} \mathrm{d}s_Q = 0 \tag{21}$$

Here n_Q and n_P are the numbers of nodes in the domains of dependence of the evaluation points Q and P, respectively. In order to numerically integrate the above BIE, the boundary of the body is discretized into a number of non-overlapping cells. Nodes are placed in each cell and the MLS interpolants can be defined in terms of the nodes alone. The cell structure can be irregular and no compatibility requirements need to be satisfied across adjacent cells. Thus the usual elemental data structure in FEM or BEM is replaced by the irregular cell structure as shown in Fig. 1a and nodes can be generated anywhere within the domain. However, the real advantages of the cell structure will become more apparent in 3-D. Regular Gaussian integration and log-weighted Gaussian integration is carried out as in Mukherjee and Mukherjee (1997a). Finally, the discretized form of eqn (21) can be written as

$$[A]\{\hat{u}\} + [B]\{\hat{\tau}\} = \{0\} \tag{22}$$

5. Application of boundary conditions

Mukherjee and Mukherjee (1997a) have imposed boundary conditions in the BNM, for potential theory, by coupling the discretized BIE in terms of approximations to the nodal variables, together with the discretized forms of the equations that relate these approximations to their actual nodal

values through MLS shape functions. For the elasticity problem at hand, an analogous procedure has been adopted in this paper. The related issue of satisfaction of the boundary conditions in the Element-Free Galerkin method has been discussed in several publications by Belytschko and his co-authors as well as in Mukherjee and Mukherjee (1997b). For a discussion of oscillatory solutions obtained from the BNM when $\hat{u}$ and $\hat{\tau}$ are not used as proposed, please see Mukherjee and Mukherjee (1997a).

Let the discretized forms of equations (15) and (16) be

$$[H]\{\hat{u}\} = \{u\} \tag{23a}$$

$$[H]\{\hat{\tau}\} = \{\tau\} \tag{23b}$$

The above equations, together with the discretized BIE (22), are rearranged by appropriate switching of columns to the forms:

$$[M_1]\{\hat{x}\} + [M_2]\{\hat{y}\} = \{0\} \tag{23c}$$

$$[H_1]\{\hat{y}\} = \{\bar{y}\} \tag{23d}$$

$$\{x\} = [H_2]\{\hat{x}\} \tag{23e}$$

where the vector $\{\bar{y}\}$ contains the prescribed boundary conditions and $\{x\}$ contains the rest. Also, $\{\hat{y}\}$ and $\{\hat{x}\}$ contain their corresponding approximations.

If N is the total number of nodes on the boundary ∂B, the BIE (23c) is a set of (dense) coupled $2N$ equations in $4N$ unknowns. Equation (23d) is another set of (sparse) $2N$ equations. One solves eqns (23c) and (23d) for the $4N$ unknowns $\{\hat{x}\}$ and $\{\hat{y}\}$ together. The overall stiffness matrix, therefore consists of $2N$ dense equations from the BIE and $2N$ sparse equations from the imposed boundary conditions.

6. Postprocessing the solution

Finally equation (23e) is used to obtain the nodal unknowns from their approximations. The last step is crucial for the success of this scheme. The approximations $\{\hat{x}\}$ are usually not accurate and often display substantial oscillations. These are damped out by postprocessing the nodal approximations with eqn (23e).

7. Handling of corners with jump discontinuities

The shape functions from MLS interpolants, and their derivatives along the boundary, are very smooth, and this could prove to be a drawback when the domain of dependence of an evaluation point extends across a corner. In potential problems, the normal derivative of the primary unknown variable suffers a jump as one crosses a corner, and it is difficult to interpolate it using MLS interpolants. Mukherjee and Mukherjee (1997a) observed oscillations in solutions of potential problems from the BNM when the domains of dependence were allowed to extend across corners. In linear elasticity, the tractions are typically discontinuous across a corner even though the displacements are continuous. If the usual scheme (without truncations) is used, oscillations are

observed both in the displacement and traction profiles even away from the corners. In order to avoid these oscillations, the domain of dependence of an evaluation point has been truncated in this work whenever it crosses a node where the normal to the boundary is discontinuous. The use of a one-sided MLS interpolant near corners substantially reduces the oscillations and this issue is discussed further in the following sections.

8. Implementation and numerical examples

The major aspects of coding for linear elasticity problems using the Boundary Node Method involve:

(a) Discretization of the geometry (boundary) into cells.
(b) Generation of node(s) in each cell.
(c) Generation of regular Gauss points and log-weighted Gauss points.
(d) Computing the domain of dependence for each evaluation point.
(e) Computation of shape functions at each node for all evaluation points.
(f) Numerical integration of the kernels in the BIE to generate the first set of $2N$ eqns (23c).
(g) Using MLS interpolants and the essential boundary conditions to generate the second set of $2N$ equations.
(h) Solution of set of equations and post processing.

Four sets of examples are illustrated in this section. All of them use the same material data as follows: Young's modulus $E = 2.5$ (in consistent units) and Poisson's ratio $v = 0.3$.

8.1. *Patch test*

In a typical patch test, a known linear displacement profile is prescribed on the boundary of the body and the displacements at interior points are computed. If the set of shape functions are consistent, the interior displacement profile will be given by the same analytical function as the one used to prescribe the boundary displacements. The patch test has been carried out on square and circular geometries and the effect of corners on the BNM solution scheme is studied.

For the BNM patch test, displacements are prescribed on the boundary ∂B. BNM solutions for boundary tractions are studied on a square plate and internal solutions for displacements are examined. The displacement boundary conditions prescribed are:

$$u^{(1)} = 2x + 3y \tag{24a}$$

$$u^{(2)} = 3x + 2y \tag{24b}$$

Ten cells, uniformly spaced, are used to discretize each segment of the square plate and two nodes are placed in each cell. In case the domain of dependence of an evaluation point is not truncated

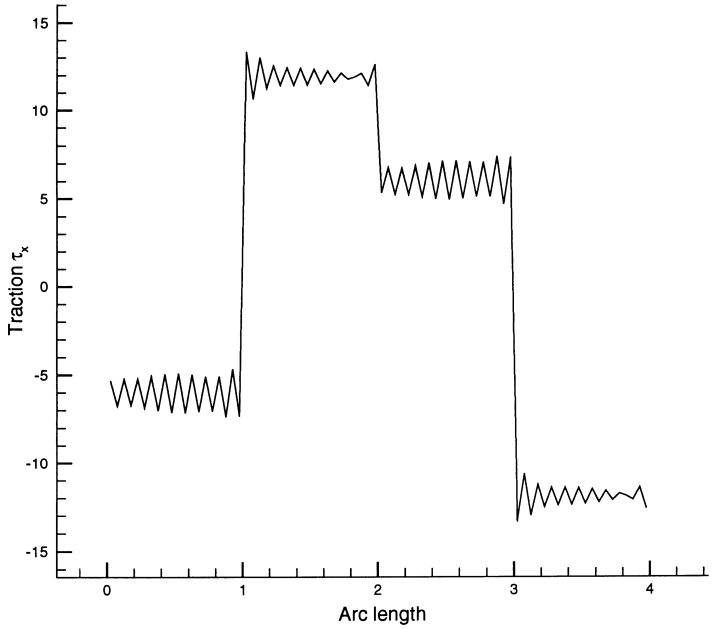

Fig. 2a. Traction distribution around the square boundary for the patch test (without truncation of domain of dependence).

at a corner, the output traction profile exhibits oscillations as shown in Fig. 2a. In case the domain of dependence is truncated at a corner, the oscillations disappear (except for sharp kinks in the cells adjacent to each corner) and the analytical solution is reproduced elsewhere [Figs 2b and c]. Since the patch test has to be exactly satisfied in order to guarantee convergence, this modification is very important. Table 1 lists the internal points and compares the computed solution with the analytical solution. For circular plates, the normal is continuous on the boundary and the usual MLS interpolants (without truncation) yield a smooth and accurate solution on the boundary and the BNM passes the patch test successfully. The BNM with truncated domains of dependence is used in the rest of the numerical examples in this paper.

8.2. *Displacement field problems*

The problem considered here is the same as described by Nagaranjan et al. (1994) and Phan et al. (1997) where it was solved using the Boundary Contour Method (BCM). Consider a circular sheet of unit radius centered at the point $(2, 2)$ in the global (x, y) coordinate system. A planar displacement profile is described on the boundary as follows:

$$u^{(1)} = \frac{x}{x^2 + y^2} \tag{25a}$$

$$u^{(2)} = \frac{y}{x^2 + y^2} \tag{25b}$$

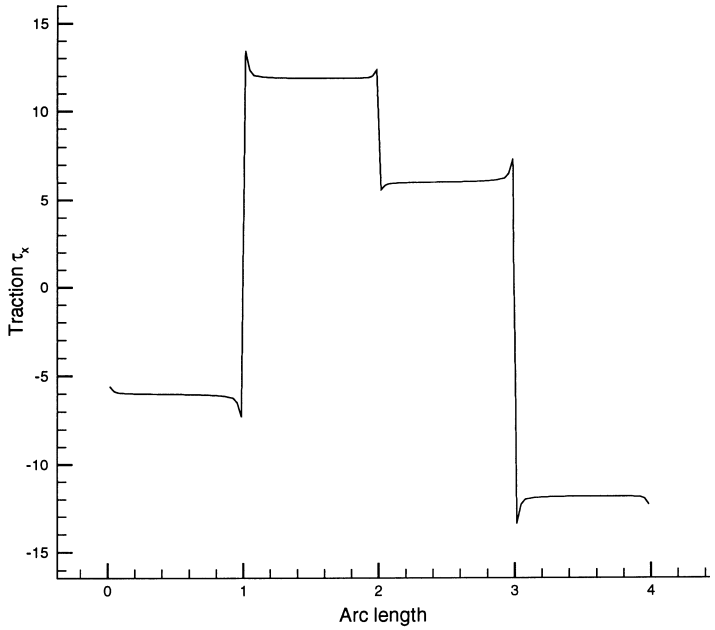

Fig. 2b. Traction distribution around the square boundary for the patch test (with truncation of domain of dependence).

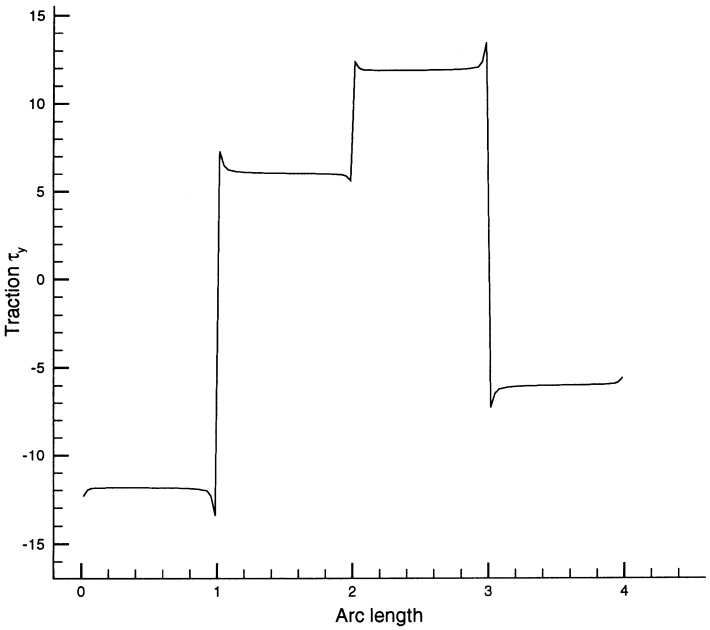

Fig. 2c. Traction distribution around the square boundary for the patch test (with truncation of domain of dependence).

Table 1
Relative errors at various locations for the patch test on a square plate. Number of cells (uniformly placed on a unit square) = 40. $\hat{d}_I = 0.25$, $c = 0.10$

Location	Error in $[u^{(1)}]$%	Error in $[u^{(2)}]$%
0.25, 0.25	0.336	0.336
0.25, 0.50	0.180	0.051
0.25, 0.75	0.116	−0.014
0.50, 0.25	0.051	0.180
0.50, 0.50	0.000	0.000
0.50, 0.75	−0.096	−0.011
0.75, 0.25	−0.014	−0.012
0.75, 0.50	−0.012	−0.027
0.75, 0.75	−0.011	−0.011

The output traction profiles along the boundary are shown in Figs 3a and b. Thirty uniform cells are used on the boundary to discretize the geometry and each cell contains two nodes. The numerical results show very good agreement with the analytical solution as shown in Figs 3a and b.

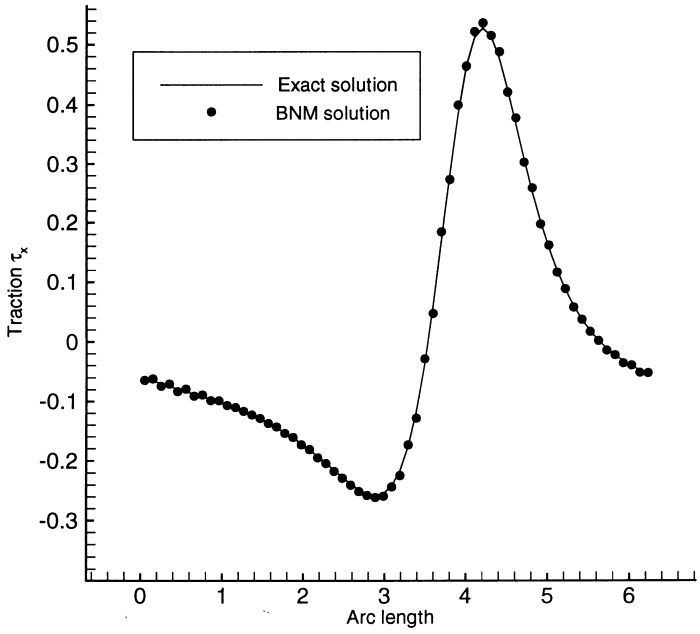

Fig. 3a. Traction distribution around the circle for the planar displacement field.

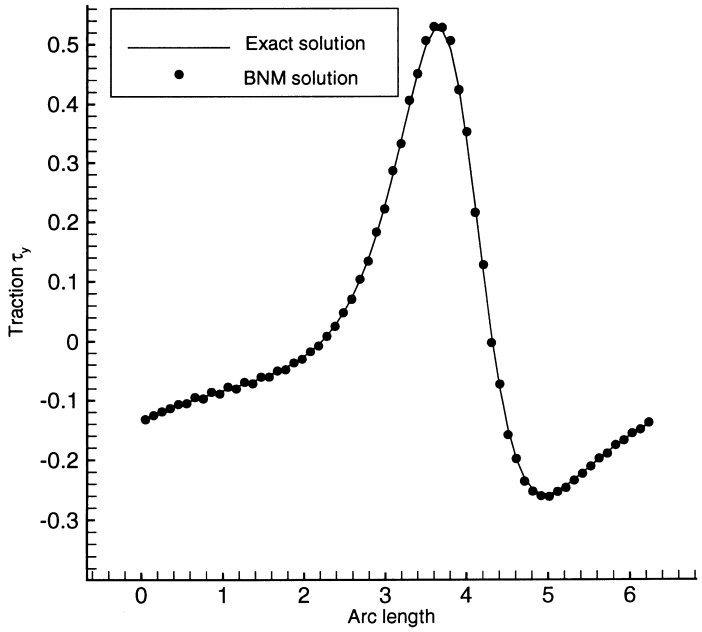

Fig. 3b. Traction distribution around the circle for the planar displacement field.

A cubic displacement profile is next prescribed on the boundary as follows:

$$u^{(1)} = y^3 - 3yx^2 \tag{26a}$$

$$u^{(2)} = -x^3 + 3xy^2 \tag{26b}$$

The numerical results for the cubic displacement also show very good agreement with the analytical solution as shown in Figs 3c and d.

8.3. *Lamé problem*

The third example involves the well known Lamé problem in which a hollow cylinder is subjected to uniform pressure on the inner surface. Let a and b denote the inner and outer radii of the cylinder, and p_i the uniform internal pressure. The stress components σ_r (in the radial direction) and σ_θ (in the circumferential direction) are given by Timoshenko and Goodier (1970)

$$\sigma_r = \frac{a^2 p_i}{b^2 - a^2}\left(1 - \frac{b^2}{r^2}\right) \tag{27a}$$

$$\sigma_\theta = \frac{a^2 p_i}{b^2 - a^2}\left(1 + \frac{b^2}{r^2}\right) \tag{27b}$$

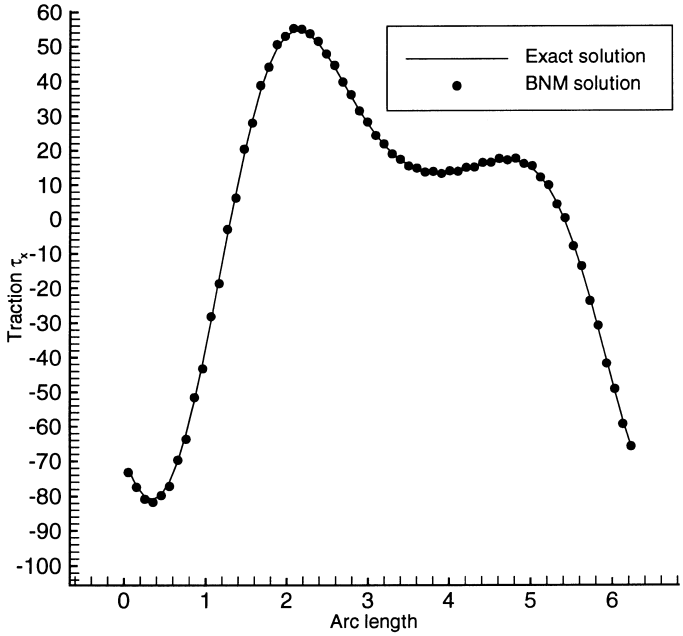

Fig. 3c. Traction distribution around the circle for the cubic displacement field.

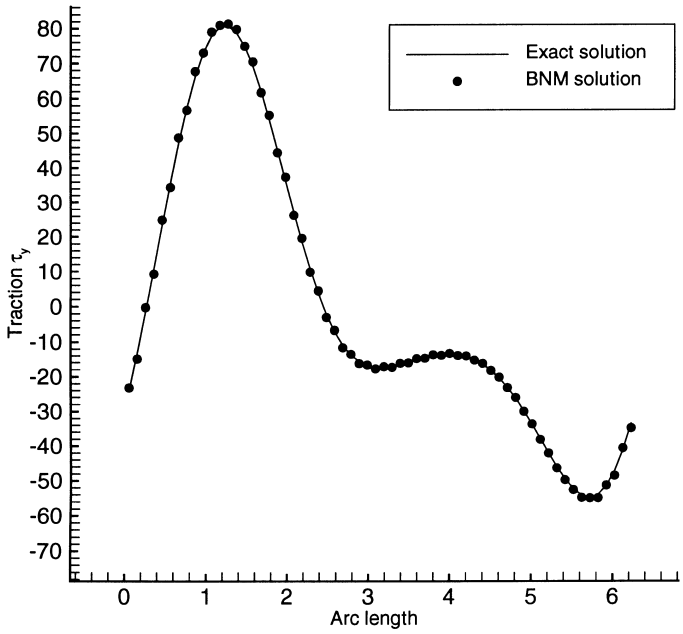

Fig. 3d. Traction distribution around the circle for the cubic displacement field.

Due to the symmetry of the problem, only a quarter of the structure is modeled as shown in Fig. 4a. Twenty uniformly placed cells are used in each boundary segment and the traction τ_y along the edge AB is shown in Fig. 4b. The numerical results are in excellent agreement with the analytical solution except for a small region around the corner where some small oscillations are observed.

8.4. *Kirsch problem*

The model for the classical Kirsch problem is shown in Fig. 5a. A total of 180 cells are used to discretize the geometry (with 40 uniform cells on AB, CD, DE and AE and 20 uniform cells along BC). In polar coordinates, the stress component σ_r in the radial direction, the stress component σ_θ in the circumferential direction and the shearing stress component $\sigma_{r\theta}$ at a point (r, θ), in an infinite plate with a circular hole, with an applied uniaxial load S, are given by Timoshenko and Goodier (1970)

$$\sigma_r = \frac{S}{2}\left(1-\frac{a^2}{r^2}\right)+\frac{S}{2}\left(1+\frac{3a^4}{r^4}-\frac{4a^2}{r^2}\right)\cos(2\theta) \tag{28a}$$

$$\sigma_\theta = \frac{S}{2}\left(1+\frac{a^2}{r^2}\right)-\frac{S}{2}\left(1+\frac{3a^4}{r^4}\right)\cos(2\theta) \tag{28b}$$

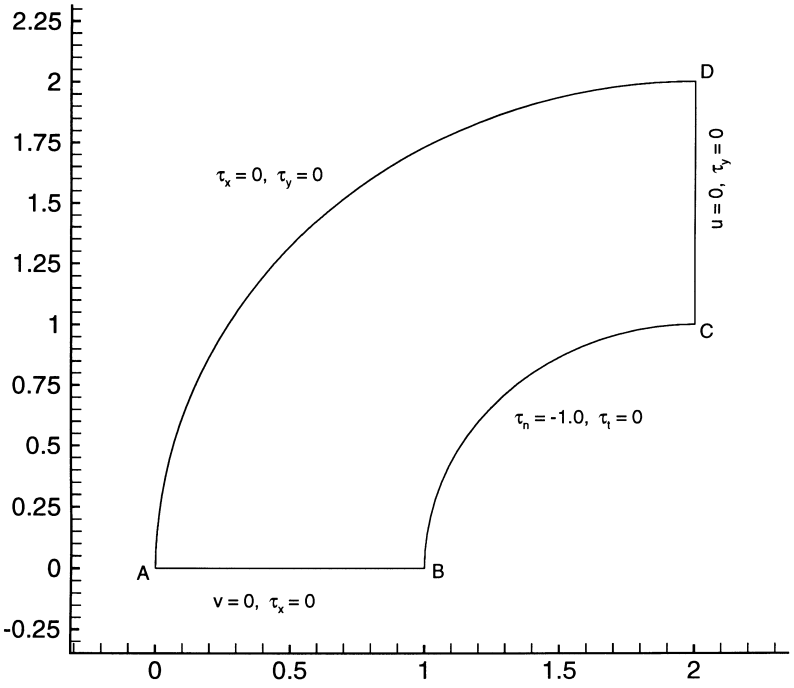

Fig. 4a. Model for the Lamé problem: uniform unit pressure distribution is prescribed along the arc BC.

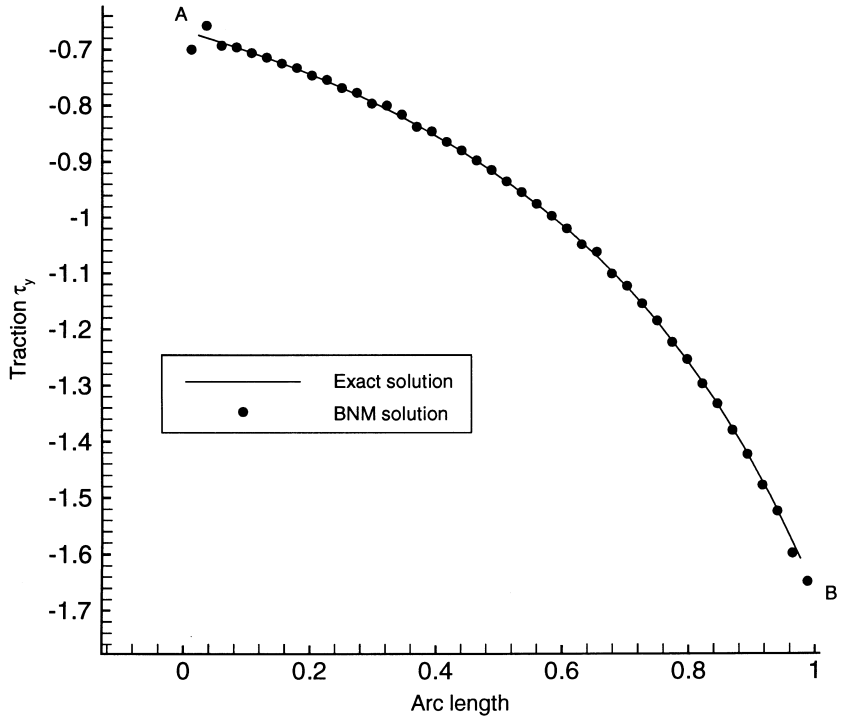

Fig. 4b. Traction distribution along the edge AB for the Lamé problem.

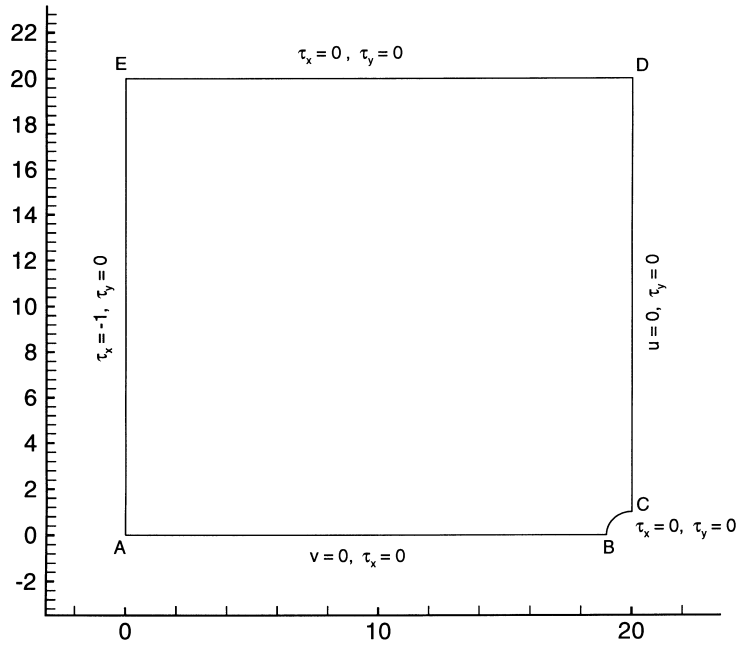

Fig. 5a. Model for the Kirsch problem: uniaxial load of magnitude $S = 1$ applied along edge AE.

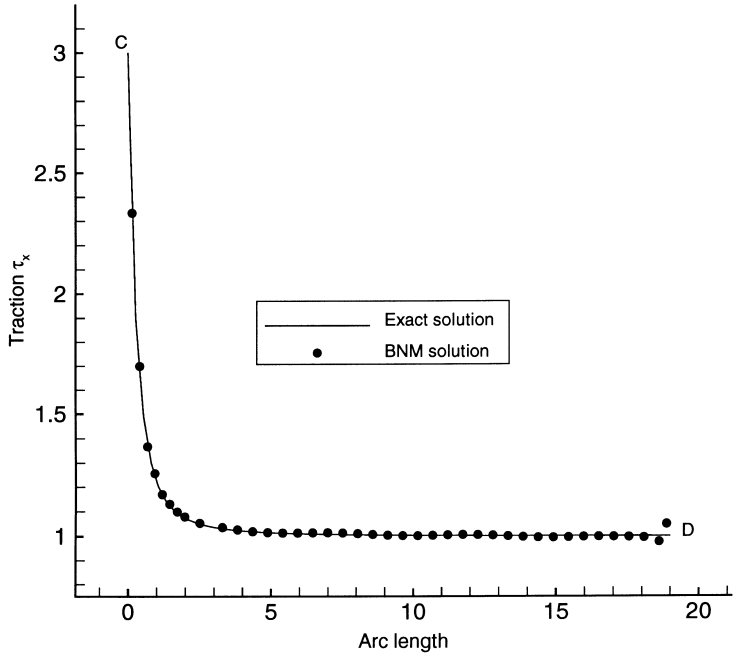

Fig. 5b. Traction distribution along edge CD for the Kirsch problem.

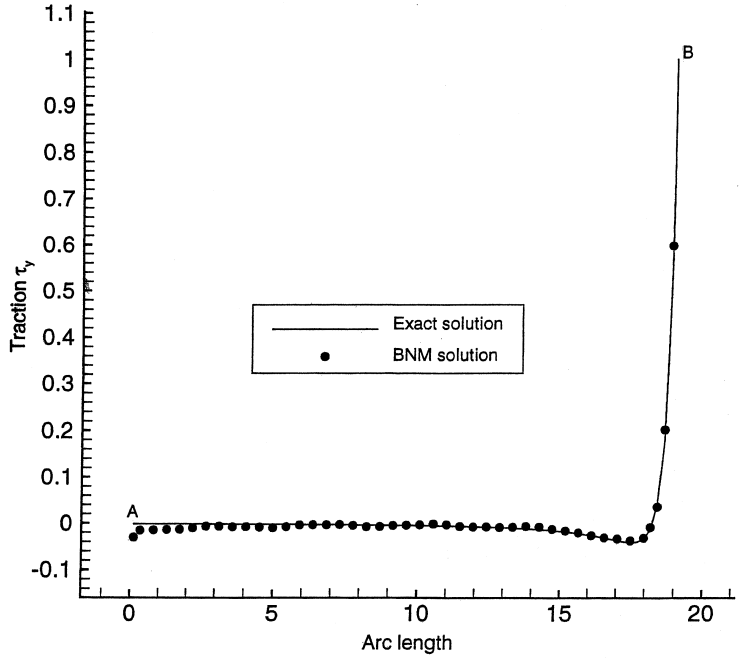

Fig. 5c. Traction distribution along edge AB for the Kirsch problem.

$$\sigma_{r\theta} = -\frac{S}{2}\left(1-\frac{3a^4}{r^4}+\frac{2a^2}{r^2}\right)\sin(2\theta) \tag{28c}$$

Along the edge CD ($\theta = \pi/2$), the traction in the x direction is given by

$$\tau_x = \frac{-S}{2}\left(2+\frac{a^2}{r^2}+\frac{3a^4}{r^4}\right) \tag{29}$$

Along the edge AB ($\theta = 0$), the traction in the y direction is given by

$$\tau_y = \frac{S}{2}\left(\frac{a^2}{r^2}-\frac{3a^4}{r^4}\right) \tag{30}$$

The Kirsch problem is more demanding than the Lamé problem due to the existence of a stress concentration at the corner C. The output traction profiles are shown in Figs 5b and c. It can be seen that the computed tractions are in good agreement with the analytical solution. Please note that in this current BNM model, there are no nodes exactly at the corners. The accuracy of these results depend on the discretization scheme and also on the parameters used to construct the weight functions, and further work is required in this area.

9. Discussion and conclusions

The initial numerical results obtained from the boundary node method for potential problems (Mukherjee and Mukherjee, 1997a), and for linear elasticity, are encouraging. The BIE have been successfully coupled with MLS interpolants and accurate numerical results have been obtained. In the work presented in this paper, the domain of dependence of an evaluation point has been modified by truncating it at corners. This procedure leads to much smoother numerical results than have been reported in Mukherjee and Mukherjee (1997a). This is a particularly useful feature for 3-D problems in which extending shape functions across boundary edges and corners might prove to be difficult. In addition, it should be noted that the same set of truncated MLS interpolants are used for interpolating both the displacement and traction components, in spite of the fact that while tractions are usually discontinuous across corners, the displacements are always continuous. In the numerical results presented here, no significant loss of accuracy has been observed due to these features. Treating the displacement and traction shape functions on an equal footing saves computational effort as compared to a scheme which employs different versions of shape functions across corners.

Acknowledgements

This research has been partially supported by a University Research Programs (URP) grant from Ford Motor Company to Cornell University.

References

Banerjee, P. K. (1994) *The Boundary Element Methods in Engineering*. McGraw-Hill, Maidenhead, Berkshire, U.K.

Belytschko, T. and Tabbara, M. (1996) Dynamic fracture using element-free Galerkin methods. *Int. J. Numer. Methods. Engrg*. **39,** 923–938.

Belytschko, T., Lu, Y. Y. and Gu, L. (1994a) Element-free Galerkin methods. *Int. J. Numer. Methods. Engrg*. **37,** 229–256.

Belytschko, T., Gu, L. and Lu, Y. Y. (1994b) Fracture and crack growth by element-free Galerkin methods. *Modeling Simul. Mater. Sci. Eng*. **2,** 519–534.

Belytschko, T., Lu, Y. Y. and Gu, L. (1995a) Crack propagation by the element-free Galerkin methods. *Eng. Frac. Mech*. 2, **51,** 295–315.

Belytschko, T., Lu, Y. Y., Gu, L. and Tabbara, M. (1995b) Element-free Galerkin methods for static and dynamic fracture. *International Journal of Solids and Structures* **32,** 2547–2570.

Belytschko, T., Krongauz, Y., Organ, D., Fleming, M. and Krysl, P. (1996) Meshless methods: an overview and recent developments. *Comput. Methods Appl. Mech. Engrg*. **139,** 3–47.

Kaljevic, I. and Saigal, S. (1997) An improved element-free Galerkin method. *Int. J. Numer. Methods. Engrg* **40,** 2953–2974.

Krongauz, Y. and Belytschko, T. (1996) Enforcement of essential boundary conditions in mesh-less approximations using finite elements. *Comput. Methods Appl. Mech. Engrg*. **131,** 133–145.

Krysl, P. and Belytschko, T. (1995) Analysis of thin plates by the element-free Galerkin method. *Comput. Mech*. **17,** 26–35.

Krysl, P. and Belytschko, T. (1996) Analysis of thin shells by the element-free Galerkin method. *International Journal of Solids and Structures* **33,** 3057–3080.

Lancaster, P. and Salkauskas, K. (1981) Surfaces generated by moving least squares methods. *Math. Comput*. **37,** 141–158.

Lancaster, P. and Salkauskas, K. (1990) *Curve and Surface Fitting—An Introduction*. Academic Press, London.

Lu, Y. Y., Belytschko, T. and Gu, L. (1994) A new implementation of the element-free Galerkin method. *Comput. Mech*. **113,** 397–414.

Mukherjee, S. (1982) *Boundary Element Methods in Creep and Fracture*. Elsevier Applied Science, London.

Mukherjee, Y. X. and Mukherjee, S. (1997a) The boundary node method for potential problems. *Int. J. Numer. Methods. Engrg*. **40,** 797–815.

Mukherjee, Y. X. and Mukherjee, S. (1997b) On boundary conditions in the element-free Galerkin method. *Comput. Mech*. **19,** 264–270.

Nagaranjan, A., Lutz, E. and Mukherjee, S. (1994) A novel boundary element method for linear elasticity with no numerical integration for 2-D and line integrals for 3-D problems. *ASME Journal of Applied Mechanics* **61,** 264–269.

Nayroles, B., Touzot, G. and Villon, P. (1992) Generalizing the finite element method: diffuse approximation and diffuse elements. *Comput. Mech*. **10,** 307–318.

Phan, A.-V., Mukherjee, S. and Rene Mayer, J. R. (1997) The boundary contour method for 2-D linear elasticity with quadratic boundary elements. *Comput. Mech*., **20,** 310–319.

Rizzo, F. J. (1967) An integral equation approach to boundary value problems of classical elastostatics. *Qly. Appl. Math*., **25,** 83–95.

Timoshenko, S. P. and Goodier, J. N. (1970) *Theory of Elasticity*. McGraw-Hill, New York, U.S.A.